Key criterion for achieving giant recovery strains in polycrystalline Fe-Mn-Si based shape memory alloys

Huabei Peng[a, b, *], Gaixia Wang[a], Shanling Wang[c, *], Jie Chen[a], Ian MacLaren[b], Yuhua Wen[a]

[a]College of Manufacturing Science and Engineering, Sichuan University, Chengdu 610065, China
[b]School of Physics and Astronomy, University of Glasgow, Glasgow G12 8QQ, United Kingdom
[c]Analytical and Testing Center, Sichuan University, Chengdu 610065, China

Abstract: In this study, it is proposed that coarsening austenitic grains is a key criterion for achieving giant recovery strains in polycrystalline Fe-Mn-Si based shape memory alloys. In order to verify the hypothesis, the relationship between recovery strains and austenitic grain-sizes in cast and processed Fe-Mn-Si based shape memory alloys was investigated. The recovery strain of cast Fe-19Mn-5.5Si-9Cr-4.5Ni alloy with the coarse austenitic grains of 652 μm reached 7.7% while the recovery strain of one with the relatively small austenitic grains of 382 μm was only 5.4%. Moreover, a recovery strain of 5.9%, which is the highest previously published value for solution-treated processed Fe-Mn-Si based shape memory alloys, was obtained by coarsening the austenitic grains through only solution treatment at 1483 K for 360 min in a processed Fe-17Mn-5.5Si-9Cr-5.5Ni-0.12C alloy. However, its recovery strain was still 5.9% after thermo-mechanical treatment consisting of 10% tensile strain at room temperature and annealing at 1073 K for 30 min. This happens because annealing twins play a negative role, refining the austenitic grains, limiting the recovery strains to below 6%. In summary, coarse austenitic grains enable the achievement large recovery strains by two mechanisms. Firstly, the grains are bigger, and consequently there are fewer grain boundaries, and thus their suppressive effects of grain boundaries on stress-induced ε martensitic transformation is reduced. Secondly, coarse austenitic grains are advantageous to introduce ε martensite with single orientation and reduce the collisions of different martensite colonies, especially when the deformation strain is large. As such, the ceiling of recovery strains is dependent on the austenitic grain-sizes.

Keywords: shape memory alloys; grain size; martensitic transformation; annealing twins

---

[*] Corresponding author. E-mail: penghuabei@scu.edu.cn (H.B. Peng); wangshanling@scu.edu.cn (S.L. Wang).

1. Introduction

Shape memory alloys (SMAs) exhibit the shape memory effect (SME) and super-elasticity, and thus are a kind of intelligent functional material combining perception and driving functions [1-6]. As such, the SMAs are promising for a wide range of applications in biomedicine, actuation, energy conversion, aerospace, robotics, civil construction, damping, and micro-electromechanical systems (MEMS), among other fields [1, 7-12]. Ni-Ti based SMAs possess an excellent SME, i.e. a large recovery strain of around 8% [13]. However, they suffer from high processing cost due to low cold workability [1, 11]. As an alternative, Fe-Mn-Si based SMAs seem to be more favorable for many applications due to their low cost, good workability, good machinability, and good weldability [14-16]. This field has emerged since Sato *et al.* discovered a giant recovery strain of 9% in a monocrystalline Fe-30Mn-1Si alloy [17]. For the purpose of practical applications, polycrystalline Fe-Mn-Si based SMAs have to be manufactured and are generally subjected to processing techniques, such as forging [18], rolling [19-21], and drawing [22]. Unfortunately, the processed polycrystalline Fe-Mn-Si based SMAs only achieve a low recovery strain of 2-3% after solution treatments at temperatures from 1273 K to 1473 K [18, 23-25]. A range of studies have, however, showed that the recovery strains could be improved up to around 5% using training, that is, several cycles of straining at room temperature (RT) and subsequent annealing at 873-923 K [25-28]. In addition to the training, the recovery strains can be enhanced significantly by thermo-mechanical treatments (TMTs), consisting of cold-rolling/deformation at RT and subsequent annealing/aging, and the aus-forming at 973 K [24-25, 29-33]. To our knowledge, however, there are no published reports of recovery strains exceeding 6% for processed polycrystalline Fe-Mn-Si based SMAs after treatments such as the training, TMTs and aus-forming.

Recently, Wen *et al.* [34] demonstrated a bending recovery strain of 8.4% and a tensile recovery strain of 7.6% in a cast and annealed polycrystalline Fe-20.2Mn-5.6Si-8.9Cr-5.0Ni alloy with coarse austenitic grains of about 1100 μm. This result was a breakthrough in attaining the large recovery strains of above 6% for polycrystalline Fe-Mn-Si based SMAs. There are two key reasons why the giant recovery strain was produced by the simple synthesis-processing of casting and annealing. One reason is that strong interactions occur between annealing twins and stress-induced ε martensite during deformation, but the formation of annealing twins is heavily suppressed by casting followed by annealing. The other is that this cast alloy primarily consisted of coarse austenitic grains. However, it is important to note that a cast

2

Fe-17.5Mn-5.29Si-9.68Cr-4.2Ni-0.09Ti alloy with small austenitic grains reached a recovery strain of just 4.5% [35]. Thus, the above results raise the question of whether coarse austenitic grains play a more crucial role than annealing twins in achieving the large recovery strains of > 6% for polycrystalline Fe-Mn-Si based SMAs.

In this paper, we test the hypothesis that coarsening austenitic grains is a key criterion for achieving a giant recovery strain in Fe-Mn-Si based SMAs. In order to do so, we produced cast Fe-Mn-Si based SMAs alloys with different sized austenitic grains by controlling the solidification rates, and then investigated the effect of austenitic grain-sizes on the stress-induced ε martensitic transformation and the recovery strains. Specifically, we investigated these effects in a processed Fe-17Mn-5.5Si-9Cr-5.5Ni-0.12C alloy and demonstrated clearly that austenitic grain-sizes determine the recovery strains but that the key parameter is the effective grain-size once the spacing of annealing twins has been taken into account.

2. Criteria of achieving giant recovery strains in polycrystalline Fe-Mn-Si based SMAs

It is beyond doubt that the SME in Fe-Mn-Si based SMAs originates from the stress-induced transformation of γ austenite to ε martensite and its reverse transformation [1]. Therefore, the basic rules for obtaining a good SME are to facilitate the stress-induced ε martensitic transformation and suppress dislocation-mediated plastic slip during deformation, as well as to promote the crystallographic reversibility of the reverse transformation on subsequent heating. To our knowledge, there are four criteria following the basic rules in published literature.

Firstly, composition design or deformation-temperature selection should be done to ensure that the stacking fault energy is as low as possible, in order to facilitate the stress-induced ε martensitic transformation. Generally, deformation mechanisms, including dislocation glide, mechanical twinning and the ε martensitic transformation, depend on the stacking fault energy in austenitic high-Mn alloys [36-37]. Studies indicate that the ε martensitic transformation can occur if the stacking fault energy is below 18 mJ/m^2; mechanical twinning can take place if the stacking fault energy is in the range of 12-35 mJ/m^2; and therefore both ε martensitic transformation and mechanical twinning can occur simultaneously when the stacking fault energy is in the range of 12-18 mJ/m^2; dislocation glide becomes the dominant deformation mechanism when the stacking fault energy is above 35 mJ/m^2 [37-41]. Therefore, for the best SME, it is necessary to ensure that the stacking fault energy is below 12 mJ/m^2 for Fe-Mn-Si based SMAs.

Secondly, a high density of stacking faults should be distributed uniformly inside the austenitic matrix

[20, 24, 31-30, 42-47]. The atomic arrangement of a stacking fault in the austenite is equivalent to a thin ε martensite with two atomic layers. As such, the stacking faults can act as embryos for the growth of ε martensite [48-49]. Therefore, the stress-induced ε martensite preferentially nucleates and grows at these pre-existing stacking faults during deformation. In this case, the critical stress inducing martensitic transformation is significantly reduced and the ability to suppress the plastic slip during stress-induced ε martensitic transformation is also enhanced. Some ways of improving the SME of Fe-Mn-Si based SMAs involve introducing a high density of uniform stacking faults *via* training, TMTs and aus-forming [24-28, 30-31, 42-47]. It should, however, be noted that reported recovery strains of processed polycrystalline Fe-Mn-Si based SMAs are still below 6%, even after the use of these methods.

Thirdly, the austenitic matrix may be strengthened through solid solution hardening with interstitial atoms such as carbon and nitrogen, or by dispersion hardening with second-phase precipitates. However, the effectiveness of carbon and nitrogen on the SME seems to be limited [50-57]. It is well known that the starting temperature of the thermally-induced martensitic transformation (M_s) can be significantly reduced by adding a small amount of carbon or nitrogen into Fe-Mn-Si based SMAs [53-54, 57]. The deformation temperature is, in most cases, at around room temperature [50-57]. Note that a good SME is generally obtained as the deformation temperature is close to the M_s [58]. As such, the strengthening effect of carbon and nitrogen on the austenitic matrix is blinded by the improper selection of deformation temperatures. As a result, the improvement of the SME is limited, and the SME may even deteriorate after the addition of carbon and nitrogen. Recently, it was found that the shape recovery ratio increased from 42% at a deformation temperature of 293 K to 81% at a deformation temperature of 77 K when the deformation strain was 3.7% in the processed Fe-17Mn-5.5Si-9Cr-5.5Ni-0.12C alloy subjected to solution treatment at 1373 K for 30 min [59]. This result clearly revealed that the addition of interstitial atoms can improve the SME of Fe-Mn-Si based SMAs radically, since the proper deformation temperature is selected. In addition to the addition of interstitial atoms, the precipitation of second-phase particles, such as NbC [25, 31, 60], VN [61-62], VC [63-64], TiC [65], and $Cr_{23}C_6$ [22], can also effectively strengthen the austenite and markedly improve the SME in Fe-Mn-Si based SMAs. Furthermore, it was reported that the precipitation of second-phase particles during the training or the TMTs is beneficial for further improving the recovery strain [66-67]. Unfortunately, polycrystalline Fe-Mn-Si based SMAs treated as above still cannot achieve the stated aim of a recovery strain more than 6%.

Fourthly, the formation of annealing twins should be suppressed in Fe-Mn-Si based SMAs [34, 68-69]. Our previous research indicated that the interactions between annealing twins and stress-induced ε martensite not only distort the twin boundaries heavily, but also significantly inhibit the stress-induced ε martensitic transformation [34]. Consequently, processed polycrystalline Fe-Mn-Si based SMAs show low recovery strains without special treatments. The number of annealing twin boundaries can be significantly reduced by training, TMTs, and aus-forming [34]. However, even then, the recovery strains cannot exceed 6% in processed polycrystalline Fe-Mn-Si based SMAs.

As summarized above, training and TMTs do not just introduce a uniformly high density of stacking faults, but also significantly reduce the amount of annealing twins. Furthermore, second-phase particles could be precipitated in the austenitic matrix after the training or the TMTs when a certain amount of carbon is added in Fe-Mn-Si based SMAs, which are beneficial for the SME. However, their recovery strains are still below 6%. In other words, it has not been possible hitherto to produce a large recovery strain of above 6% only based on the above four criteria. The reason for this may be associated with the austenitic grain-size. In general, it is easy to reach austenitic grain-sizes of about 500 μm, even millimeter-scale, by casting. However, the austenitic grain-sizes are generally below about 200 μm in processed Fe-Mn-Si based SMAs. In this case, a large recovery strain of above 6% can be obtained in cast Fe-Mn-Si based SMAs, whereas, the processed Fe-Mn-Si based SMAs cannot achieve such a high level of recovery strains. It may, therefore, be hypothesized that the maximum recovery strain is dependent on the austenitic grain-size for polycrystalline Fe-Mn-Si based SMAs. Consequently, we propose that austenitic grain growth is a key step towards achieving giant recovery strains in Fe-Mn-Si based SMAs, in addition to the above four criteria.

3. Materials and methods

The chemical compositions of the cast and processed Fe-Mn-Si-Cr-Ni SMAs investigated in this work are listed in Table 1. In an induction furnace with an argon atmosphere, the cast alloys were melted and then poured into a mould of sodium silicate sand. Generally, cast Fe-based alloys with different grain-sizes can be obtained by two ways: controlling solidification rate and adding grain refining elements. In the present paper, we cast $20 \times 130 \times 150$ mm^3 and $5 \times 130 \times 150$ mm^3 plates simultaneously to achieve two different solidification rates, and thus two cast Fe-Mn-Si-Cr-Ni SMAs with identical chemical compositions but different initial grain-sizes were attained. In order to distinguish the two cast plates with 5

mm and 20 mm thickness, they are denoted the 19Mn-5 alloy and 19Mn-20 alloys, respectively. The processed Fe-17Mn-5.5Si-9Cr-5.5Ni-0.12C alloy was also melted in a vacuum induction furnace under an argon atmosphere. The ingot was hot rolled at 1423 K into plates after homogenization treatment at 1373 K for 12 h. Then, the plates were cold rolled with a thickness reduction of 20% to 2.2 mm. All specimens were prepared by wire electrical discharge machining.

For further improving the SME, the cast alloys were annealed at 873 K for 30 min. In order to obtain different austenitic grain-sizes, the processed alloy was solution-treated at 1373 K for 30 min, 1473 K for 120 min and 1483 K for 360 min, respectively. In addition, the solution-treated specimens were further subjected to a TMT consisting of 10% tensile strain at RT and annealing at 1073 K for 30 min.

The SME was tested by a conventional bending technique, and the details of this technique were shown in our previous paper [28]. Specimens with 1.5 mm thickness were used for the bending tests. Moreover, the specimens were deformed at a temperature of M_s + 10 K. Additionally, solution-treated Fe-17Mn-5.5Si-9Cr-5.5Ni-0.12C samples were deformed in bending at 77 K because their M_s did not appear after cooling to 77 K.

Specimens were mechanically ground and then electro-polished in an electrolyte consisting of 10% perchloric acid and 90% ethanol before metallographic and EBSD observation. A conventional etchant, consisting of 1 g oxalic acid, 15 ml hydrogen peroxide, 1 ml hydrogen fluoride, and 15 ml distilled water, was used to reveal solidification structures [70]. For the purpose of characterizing morphology of austenitic grains, a tint etchant was selected and composed of 0.5 g potassium metabisulfite, 20 g ammonium bifluoride and 100 ml distilled water [71]. In addition, another tint etchant, 1.2% potassium metabisulfite and 0.5% ammonium bifluoride in distilled water, was used to determine different phases. In the color optical micrographs, austenite appears brown and ε martensite appears white after etching with this etchant, except that thin plates appear as dark lines [72]. We used Analysis Five software (Olympus, Japan) to montage the optical micrographs to create high-resolution large-area images of the coarse-grained cast alloys. The mean grain-size was determined by using a linear intercept method on three lines [73], and the observed area was 16 mm^2 at least. The volume fraction of stress-induced ε martensite was determined by a manual point count: an array of one thousand points formed by a grid, which consists of equally spaced points formed by the intersection of fine lines, is superimposed upon a large color optical micrograph. The volume fraction of stress-induced ε martensite equals that the number of points falling on the ε martensite is

divided by the total number of points in the array. Specimens were also characterized using JEOL 6500F and FEI F50 scanning electron microscopes (SEMs) equipped with electronic backscatter diffraction (EBSD) systems. Step sizes of 0.9 μm and 5 μm were used for EBSD scans of the processed and cast samples, respectively. Resistivity-temperature curves were measured to obtain phase transformation temperatures. In order to determine the temperature dependence of 0.2% proof-stress, tensile tests were carried out at different temperatures.

4. Verifying the key criterion of achieving giant recovery strains

4.1 Effect of solidification rates on grain-sizes

The famous Chvorinov rule [74] is a powerful method describing the freezing time of a casting with simple shape according to the expression

$$t = B\left(\frac{V}{A}\right)^2 \qquad [1]$$

where t is the total freezing time, B is a constant for given metal and mold conditions, V is the volume of the casting, and A is the area of the metal-mold interface. For as-cast 19Mn-5 and 19Mn-20 alloys, B is same, and the values of V and A are known. Thus, the ratio of the freezing time of the 19Mn-20 alloy to that of the 19Mn-5 alloy is about eleven because the two cast alloys were cast at the same time. In other words, the solidification rate of the 19Mn-5 alloy is about eleven times than that of the 19Mn-20 alloy.

Fig. 1 shows the solidification microstructures of as-cast 19Mn-5 and 19Mn-20 alloys. Our previous results showed that the 19Mn-20 alloy solidified as ferritic mode, and thus its as-cast microstructure is the typical Widmanstätten morphology [70]. The as-cast microstructure also displays an Widmanstätten morphology for the 19Mn-5 alloy, and its solidification mode is therefore also ferritic mode. If the solidification mode of cast Fe-Mn-Si based SMAs is ferritic mode, the liquid phase will first transform into primary δ ferrite completely, and the austenite will subsequently grow into the primary δ ferrite from its grain boundaries by Widmanstätten mechanism during cooling [70, 75-76]. In this case, the grain boundaries of primary δ ferrite can be revealed clearly in the ordinary optical micrographs (dotted lines), as seen in Fig. 1. The mean grain-size of primary δ ferrite is 727 μm in the as-cast 19Mn-5 alloy, and it is 1242 μm for the as-cast 19Mn-20 alloy. The grains of primary δ ferrite in the as-cast 19Mn-5 alloy are smaller than those in the as-cast 19Mn-20 alloy because the former solidification rate is higher than the latter one during the solidification process.

7

Fig. 2 reveals the austenitic grain morphology of as-cast 19Mn-5 and 19Mn-20 alloys. The morphology of austenitic grains is irregular rather than regular polygonal in the as-cast 19Mn-5 and 19Mn-20 alloys. In Fe-Mn-Si based SMAs with the ferritic mode, a majority of the primary δ ferrite will transform into the austenite after the liquid phase completely transforms into the primary δ ferrite [70, 75-76]. Thus, these irregular austenitic grains result from $\delta \rightarrow \gamma$ phase transformation. Furthermore, the austenitic grains are smaller in the as-cast 19Mn-5 alloy than in the as-cast 19Mn-20 alloy. The reason for this result is that the grains of primary δ ferrite for the as-cast 19Mn-5 alloy were refined due to higher solidification rate as compared with the as-cast 19Mn-20 alloy.

Fig. 3 compares austenitic crystallographic orientation maps and corresponding grain maps for as-cast 19Mn-5 and 19Mn-20 alloys after annealing at 873 K for 30 min. The crystallographic texture is weak for both cast alloys. The austenitic grain morphology is same before and after annealing, i.e. irregular grain boundaries. According to the results of EBSD, the mean austenitic grain-size of the 19Mn-5 alloy is 382 μm while that of the 19Mn-20 alloy is 652 μm. The former austenitic grain-size is still smaller for the faster cooled 19Mn-5 alloy than for the 19Mn-20 alloy after annealing.

4.2 Effect of grain-sizes on stress-induced martensitic transformation

When the deformation temperature is close to M_s, it is easy for stress-induced ε martensite to be induced while it is difficult for permanent slip to be introduced [58]. As a result, a good SME can be obtained if the deformation temperature is at around the M_s. Accordingly, we deformed as-cast 19Mn-5 and 19Mn-20 alloys annealed at 873 K for 30 min at $M_s + 10$ K and investigated the effect of grain-sizes on the stress-induced ε martensitic transformation. Table 2 gives their phase transformation temperatures.

Fig. 4 shows the color optical micrographs of as-cast 19Mn-5 and 19Mn-20 alloys annealed at 873 K for 30 min after 5% deformation at $M_s + 10$ K. For the 19Mn-5 alloy, the stress-induced ε martensitic transformation occurred uniformly in almost every austenitic grain, and two orientations of stress-induced ε martensite were induced at least in one austenitic grain, as shown in the Region Ⅰ of Fig. 4. However, the ε martensite was induced unevenly for the 19Mn-20 alloy. One dominant orientation of ε martensite was induced in some austenitic grains, such as Regions Ⅱ and Ⅳ. On the contrary, there were two or more orientations of ε martensite in some austenitic grains, especially in the relatively small austenitic grains, as seen in the Regions Ⅱ and Ⅲ. Different amount of ε martensite were induced in different austenitic grains,

and more ε martensite was induced in the bigger austenitic grains, as shown in the Regions Ⅱ and Ⅳ. In addition, there is more stress-induced ε martensite in the Region Ⅳ than in the Region Ⅲ for the same austenitic grain. On the whole, the amount of stress-induced ε martensite is more for the 19Mn-20 alloy than for the 19Mn-5 alloy after 5% deformation.

Figs. 5 and 6 show the color optical micrographs of as-cast 19Mn-5 and 19Mn-20 alloys annealed at 873 K for 30 min after 10% deformation at M_s + 10 K, respectively. For the 19Mn-5 alloy, just one dominant orientation of ε martensite was induced in some austenitic grains (Region A), but two or more orientations of ε martensite were appeared in other austenitic grains. In some junctional corners of austenitic grains, two orientations of ε martensite collided with each other, such as Region B. For the 19Mn-20 alloy, one dominant orientation of ε martensite was induced in a majority of austenitic grains, especially coarse austenitic grains (Regions C and D). Furthermore, the single orientation of ε martensite was induced in the junctional corner, as indicated by the loop in the Region C. Note that the volume fraction of stress-induced ε martensite is also more for the 19Mn-20 alloy than for the19Mn-5 alloy after 10% deformation.

4.3 Effect of grain-sizes on temperature dependence of 0.2% proof-stress

Fig. 7 shows the temperature dependence curves of 0.2% proof-stress for as-cast 19Mn-5 and 19Mn-20 alloys annealed at 873 K for 30 min. These curves are composed of a straight dashed line with positive slope and a straight full line with negative slope. Similar results have also been reported by many researchers [26, 55-56, 77-82]. The dashed line with positive slope represents the critical stress to induce martensitic transformation, and the full line with negative slope indicates the critical stress for plasticity with irrecoverable slip. Since the stress is within the area between the straight full and dashed lines, the stress-induced martensitic transformation can occur preferentially. When the stress is above the full line, the plasticity with irrecoverable slip must be activated. For polycrystalline materials, the classical Hall-Petch relationship [83] can be used to describe the effect of grain-size on the yield stress *via* slip of dislocations in the well-known equation:

$$\sigma = \sigma_0 + kd^{-0.5} \tag{2}$$

where σ is the yield stress, σ_0 is often identified with "friction stress" needed to move individual dislocations during deformation, k is a constant often referred to as the Hall-Petch slope and is material

dependent, and d is the average grain-size. Based on the Hall-Petch relationship, the yield strength of materials can be significantly improved by grain refinement. Therefore, the yield stress is higher in the 19Mn-5 alloy than in the 19Mn-20 alloy (full lines with positive slope) because the austenitic grains are much smaller in the former alloy than in the latter one. Furthermore, the slope of the dashed line is smaller for the 19Mn-5 alloy than for the 19Mn-20 alloy. That is, the critical stress to induce martensitic transformation declines more quickly with decreasing temperature for the 19Mn-20 alloy than for the 19Mn-5 alloy. This result reveals that grain refinement increases the critical stress to induce the martensitic transformation and suppresses the stress-induced martensitic transformation. In addition, $\Delta\sigma$ is the difference between the extrapolated yield stress and the critical stress to induce martensitic transformation at a certain temperature (which in this paper is taken as $M_s + 10$ K). It is regarded as a measure of the degree of plastic slip suppression during stress-induced ε martensitic transformation. If $\Delta\sigma$ is larger, then the plastic slip is less likely under deformation [26, 55-56, 78]. $\Delta\sigma$ at $M_s + 10$ K for the 19Mn-5 alloy is smaller than that for the 19Mn-20 alloy. Thus, plastic slip suppression during stress-induced ε martensitic transformation is weaker for the 19Mn-5 alloy than for the 19Mn-20 alloy at $M_s + 10$ K, even if grain refinement strengthens the austenite for the 19Mn-5 alloy. The result indicates that the ability to suppress the plastic slip during stress-induced ε martensitic transformation could be enhanced by coarsening the austenitic grains for cast Fe-Mn-Si based SMAs.

4.4 Effect of grain-sizes on shape memory effect

Fig. 8 shows the effect of deformation strains on the recovery strains of as-cast 19Mn-5 and 19Mn-20 alloys after annealed at 873 K for 30 min. The recovery strain of the 19Mn-5 alloy increases with increasing the deformation strains but reaches a maximum value of 5.4% at around 8.7%, beyond which its recovery strain decreases. In contrast to this, the recovery strain of the 19Mn-20 alloy continues to increase with increasing deformation strains up to the highest strains used in the test such that, when the deformation strain reaches 13%, its recovery strain reaches 7.7%. Consequently, the 19Mn-20 alloy is increasingly superior to the 19Mn-5 alloy in this respect with increasing deformation strain.

4.5 Discussion

The volume fractions of stress-induced ε martensite are lower in 19Mn-5 alloy with small austenitic grains than in 19Mn-20 alloy with coarse austenitic grains after 5% or 10% deformation at $M_s + 10$ K (Figs.

4-6). Furthermore, the volume fraction difference of stress-induced ε martensite between the 19Mn-5 and 19Mn-20 alloys increases from 13% to 22% when the deformation strain increases from 5% to 10%. From these results, it is demonstrated that coarse austenitic grains are more beneficial for the stress-induced ε martensitic transformation as compared with small austenitic grains during deformation, especially when the deformation strains are large. In addition, the result of the temperature dependence of 0.2% proof-stress in Fig. 7 further reveals that the ability to suppress the plastic slip during stress-induced ε martensitic transformation is weaker in the 19Mn-5 alloy than in the 19Mn-20 alloy when deformed at $M_s + 10$ K. Thus, there is no doubt that coarse austenitic grains are more conducive to the stress-induced ε martensitic transformation than small austenitic grains. An increase in austenitic grain-sizes would result in decreasing the density of grain boundaries. Obviously, the density of grain boundaries has a significant effect on the stress-induced ε martensitic transformation.

On the one hand, Ueland and Schuh [84] reported that grain boundaries have a strong effect on the stress-induced martensitic transformation in Cu-Zn-Al SMA, by use of experiments on microwires containing a small amount of grains and grain junctions. In the regions away from grain boundaries, the austenite was fully transformed into martensite. In the regions around grain boundaries, however, untransformed austenite appeared and the stress-induced martensitic transformation was partial. Therefore, grain boundaries have an inhibiting effect on the martensitic transformation. In the present case, the regions near grain boundaries would be expected to show reduced transformation into ε martensite. As such, if the grains are bigger, there is a larger proportion of the sample available for stress-induced ε martensitic transformation.

Prior studies have also indicated that grain-size influences the martensitic transformation temperature in SMAs. Takaki $et\ al.$ [85] reported that the M_s increased with increasing the austenitic grain-sizes from 4 μm to 130 μm in a Fe-15Mn alloy. Jun and Choi [86] obtained a similar result in a Fe-18Mn alloy with the austenitic grain-sizes from 13 μm to 185 μm. In addition to Fe-Mn alloys, M_s also decreased with the grain-sizes for grain-sizes below 100 μm in polycrystalline Fe-Ni-C [87-89], Fe-Pd [90], Cu-Zn-Al [91], Cu-Al-Ni [92] and Cu-Al-Mn [93] SMAs. Even more seriously, Waitz $et\ al.$ [94] found that the martensitic transformation is no longer observed in Ni-Ti alloy below a critical grain size around 50 nm. In the present paper, it is also found that the M_s of 19Mn-5 alloy with small austenitic grains is also lower than that of 19Mn-20 alloy with coarse austenitic grains (Table 2). Thus, the thermally-induced martensitic

11

transformation is suppressed after grain refinement. Additionally, the stress-induced martensitic transformation is also inhibited due to grain refinement. In Fe-Mn-Si based [95-96], Cu based [73, 97-99] and Ni-Ti based [100] alloys, the critical stress to induce martensitic transformation increases with decreasing the grain-sizes. Our present results also reveal that the critical stress to induce martensitic transformation is also higher in 19Mn-5 alloy than in 19Mn-20 alloy (Fig. 7). From all these cases, it is concluded that the refinement of the grain-sizes inhibits the growth of martensite from the austenite matrix.

Sinclair *et al.* [101-102] built the correlation between role of back-stress (σ_B) provided by dislocations and grain-size (*d*) for copper alloys *via* the following equation

$$\sigma_B = M \frac{Gb}{d} n \qquad [3]$$

where *M* is the Taylor factor, *G* is the shear modulus, *b* is the magnitude of the Burgers vector, and *n* is the number of dislocations present at a grain boundary on a given slip system. According to this equation, the back-stress decreases with increasing the grain-sizes. In the case of Fe-Mn-Si based SMAs, a decrease in austenitic grain-sizes would result in severely limiting the growth of ε martensite in the regions around grain boundaries *via* the resulting increase of back-stress from grain boundaries. In other words, the decrement of the grain-size enhances the suppressive effect of grain boundaries on the stress-induced ε martensitic transformation.

In addition, in order to overcome the increased back-stress from grain boundaries with decreasing the grain-size described by Eq. [3], a larger driving force is required for the martensitic transformations. As a result, the M_s decreases and the critical stress to induce the martensitic transformation increases with decreasing the austenitic grain-sizes. Furthermore, the critical stress to induce the martensitic transformation declines more quickly with decreasing temperature in 19Mn-5 alloy than in 19Mn-20 alloy, while the yield stress difference between these two alloys is almost constant over a range of temperature. That is, the increment of the critical stress to induce martensitic transformation is bigger than the increment of the yield stress after grain refinement. This indicates that the austenitic grain-sizes exhibit a more drastic effect on the critical stress to induce martensitic transformation than the yield stress. Therefore, during stress-induced ε martensitic transformation, the ability to suppress the plastic slip declines owing to grain refinement for the 19Mn-5 and 19Mn-20 alloys.

The transformation from austenite to ε martensite is realized by the motion of one a/6<112> Shockley

partial dislocation on every second (111) austenite plane in Fe-Mn-Si based SMAs [1]. In this case, twelve martensite variants correspond to twelve shear systems. However, only four groups of martensite corresponding to the $\{111\}_\gamma$ with four planes could be observed because variants with a common basal plane generally look like a parallel band. Thus, four orientations of ε martensite could be seen in Fe-Mn-Si based SMAs. In polycrystalline metals, five independent shear systems exist during deformation [103]. It is important to note that in order to satisfy the requirement of boundary compatibility, these shear systems may be fully or partly activated, which is associated with the grain-size [103]. If the grain is coarse enough, only one shear system may be activated because the areas affected by grain boundaries are much less. Otherwise for smaller grains, two or more shear systems must be activated because the volumes affected by grain boundaries are a higher fraction of the total. In the case of Fe-Mn-Si based SMAs, coarse austenitic grains are advantageous to introduce the ε martensite with single orientation, whereas two or more orientations of ε martensite have to be introduced in relatively small austenitic grains, owing to meet the requirement of boundary compatibility lying on the austenitic grain-sizes. It is indirectly demonstrated by the results reported by Ueland *et al.* [84] that single orientation martensite was induced in the regions near single grain boundary, while multiple-orientations of martensite were induced in the regions around a triple junction in Cu-Zn-Al shape memory microwires. For 19Mn-5 alloy with small austenitic grains, two orientations of stress-induced ε martensite were induced at least in one austenitic grain after 5% deformation (Fig. 4). However, one dominant orientation of ε martensite appears in some coarse austenitic grains, while two or more orientations of ε martensite were introduced in some relatively small austenitic grains for 19Mn-20 alloy with coarse austenitic grains. Furthermore, in the 19Mn-20 alloy one dominant orientation of ε martensite was induced in a majority of austenitic grains, especially coarse austenitic grains, when the deformation strain raised to 10% (Fig. 6). The above results further reveal that the number of orientations for stress-induced ε martensite is dependent on the austenitic grain-sizes. That is, coarse austenitic grains are advantageous to induce single orientation ε martensite. In some junctional corners, two orientations of ε martensite collided with each other for the 19Mn-5 alloy after 10% deformation, while single orientation ε martensite was introduced for the 19Mn-20 alloy (Figs. 5 and 6). This result indicates that the formation of two or more orientations of ε martensite in junctional corners could be suppressed since the austenitic grains are big enough. Accordingly, there are more collisions in the 19Mn-5 alloy with

13

small austenitic grains than in the 19Mn-20 alloy with coarse austenitic grains after deformation, particularly when the deformation strain was 10%. Studies clearly revealed that the collisions between different orientation ε martensite suppress the stress-induced ε martensitic transformation and lead to a poor SME for Fe-Mn-Si based SMAs [104-105]. Thus, as compared with small austenitic grains, coarse austenitic grains are more conducive to the stress-induced ε martensitic transformation because the single orientation ε martensite is favorable to be induced, especially when the deformation strain is large. This is the reason why the recovery strains of the 19Mn-20 alloy are increasingly larger than those of the 19Mn-5 alloy with increasing the deformation strains (Fig. 7).

To sum up, there are two roles of coarse austenitic grains in facilitating the stress-induced ε martensitic transformation. Firstly, the grains are bigger, the amount of grain boundaries is less, and thus their regions suppressing stress-induced martensitic transformation are a smaller proportion of the total grain volume. Secondly, the collisions between different orientation ε martensite suppress the stress-induced ε martensitic transformation, and coarse austenitic grains are therefore beneficial as these allow the formation of single orientation of ε martensite and reduce the collisions from differently nucleated martensite orientations, especially when the deformation strain is large. Therefore, the key criterion of producing coarse austenitic grains has to be obeyed for the purpose of achieving giant recovery strains in Fe-Mn-Si based SMAs. To obtain cast Fe-Mn-Si based SMAs with giant recovery strains, the design of casting parameters and the addition of alloying elements must follow this key criterion. For example, the solidification rate should be as small as possible, and alloying elements that result in grain refinement should not be introduced.

5. Attempt to obtain giant recovery strains by following the key criterion in processed Fe-Mn-Si based SMAs

5.1 Coarsening austenitic grains

A 20% cold-rolled Fe-17Mn-5.5Si-9Cr-5.5Ni-0.12C alloy was chosen to further demonstrate our proposal that coarsening austenitic grains is a key criterion of achieving giant recovery strains in Fe-Mn-Si based SMAs. First, the austenitic grains should be coarsened as much as possible. It is well known that heating treatment is a simple way to adjust the grain-sizes of metals and alloys. The grain-sizes have a strong correlation with heating temperature and heating time, as shown in the following equation [106]

$$d^m = d_0^m + k_0 t \exp(-\frac{Q}{RT}) \qquad [4]$$

where d is the final grain-size, d_0 is the initial grain-size, m is the grain growth exponent and k_0 is the fitting

constant, t is the heating time, T is the heating temperature, Q is the activation energy for boundary mobility,

and R is the gas constant. According to the Eq. [4], raising the heating temperature and extending the

heating time are expected to coarsen the grain-size. For the purpose of obtaining the coarse austenitic grains,

the processed alloy was solution-treated at 1473 for 120 min and 1483 K for 360 min, respectively. By way

of contrast, some specimens of the processed alloy were solution-treated at 1373 K for 30 min to obtain

smaller austenitic grains.

Fe-Mn-Si based SMAs are face-centred cubic (FCC) metals with low SFE. As such, lots of annealing

twins can be observed after cold working followed by annealing. Such twin boundaries may be considered

as a barrier to dislocation motion just as for grain boundaries [83, 107]. In addition, previous studies

revealed that the stress-induced ε martensite collides with the twin boundaries during deformation

preventing the propagation of the stress-induced ε martensite [34]. In this case, an effective austenitic

grain-size (D_{eff}) should be introduced, taking into account the existence of twin boundaries. If a twin

boundary is considered as a grain boundary, the D_{eff} of the processed alloy subjected to solution treatment at

1373 K for 30 min was 41.7 μm, whereas the austenitic grain-size without considering the twin boundaries

(D) was 87.9 μm, as shown in Fig. 9 (a) and Table 3. Thus, the effective austenitic grain-size is hugely

affected by the inclusion of the annealing twins in the calculation. After further TMT consisting of 10%

tensile strain at RT and annealing at 1073 K for 30 min, a large number of interfaces appear similar to

annealing twins but cannot be identified as twin boundaries since the tolerance value for the misorientation

of the twin is set as 5° in the TSL OIM software, as seen in Fig. 9 (b). Our previous quasi *in situ* EBSD

results indicated that the misorientation across many straight interfaces is $>$ 65°or $<$ 55° [34]. As such,

they can be supposed to be the distorted twin boundaries which also exhibit the effect of grain refinement.

In this case, the D_{eff} was 53.1 μm while the D was 104.2 μm for the processed alloy subjected to the TMT.

In addition, the corresponding D_{eff} and D for solution-treated processed alloy at 1483 K for 360 min as well

as one subjected to the TMT can be obtained, as seen in Table 3. The austenitic grains are much bigger in

the solution treated alloy at 1483 K for 360 min than in that at 1373 K for 30 min before and after the TMT,

as shown in Table 3 and Fig. 10.

5.2 Recovery strains before and after coarsening austenitic grains

M_s temperatures did not appear after even cooling to 77 K for solution-treated Fe-17Mn-5.5Si-9Cr-5.5Ni-0.12C samples, while they were observed in the case of thermo-mechanically treated ones (Table 4). The maximum recovery strain of processed Fe-17Mn-5.5Si-9Cr-5.5Ni-0.12C alloy subjected to solution treatment at 1373 K for 30 min reaches 4.2%. In the case of the processed alloy subjected to solution treatment at 1483 K for 360 min, it is worth noting that its maximum recovery strain further increased to 5.9%, which is bigger than the maximum recovery strain of 5.6% for the processed alloy subjected to the solution treatment at 1373 K for 30 min and TMT. The value of 5.9% is the highest recovery strain among solution-treated processed Fe-Mn-Si based SMAs published to date. As such, the above results further confirm that coarsening austenitic grains is the key criterion that must be fulfilled in order to achieve giant recovery strains in polycrystalline Fe-Mn-Si based SMAs. Additionally, the recovery strain was only improved by further TMT when the deformation strains were below 9% for the processed alloy subjected to the solution treatment at 1483 K for 360 min. However, the maximum recovery strain had no change and was 5.9% before and after TMT. This result indicates that the effectiveness of TMTs is dependent on the austenitic grain-size. In other words, the austenitic grain-size is the key factor determining the ceiling of recovery strains in polycrystalline Fe-Mn-Si based SMAs. In previous publications on processed Fe-Mn-Si based SMAs, the highest heating temperature was 1473 K, as reported by Kajiwara and co-workers in several Fe-Mn-Si SMAs containing Nb and C [25, 31, 46, 60, 79, 108]. However, Nb inhibits the growth of austenitic grains. In this case, although the heating temperature was as high as 1473 K, the growth of austenitic grains is restricted owing to the effect of Nb (possibly either by Nb segregation on grain boundaries or grain refinement by NbC precipitation). Therefore, these Fe-Mn-Si SMAs containing Nb element cannot exhibit a large recovery strain of above 6% after TMTs accompanied by the precipitation of NbC particles [25, 60]. In the present paper, the maximum effective austenitic grain-size is only 185.5 μm. As such, data on the recovery strains of the processed polycrystalline Fe-Mn-Si based SMAs are not beyond 6%. However, it is expected that the recovery strain of above 6% may be obtained through further coarsening the austenitic grains in processed Fe-Mn-Si based SMAs.

5.3 Limitation of coarsening austenitic grains by solution treatments

As mentioned above, since a twin boundary is considered as a grain boundary, the relationship between D_{eff} and D can be described by the following equation:

$$D_{eff} = \frac{D}{[1+N]} \qquad [5]$$

where N is the number of twin boundaries per grain. Furthermore, Pande *et al.* [83, 109] provided an equation to describe the relationship between n (the number of twins per grain) and D, as follows:

$$n = K_t \ln(\frac{D}{D_0}) \qquad [6]$$

where K_t is a constant and D_0 is the minimum grain-size below which no twin boundaries may exist. Note that four types of annealing twins are observed in FCC crystals [110], as shown in Fig. 11. Obviously, only C-type twins in Fig. 11 possess two independent twin boundaries and divides one grain into three parts. In this case, $N = pn$, where p is a correction factor which is dependent on the density of C-type twins, and $1 \leq p \leq 2$. Therefore, according to Eqs. [5] and [6], the relationship between D_{eff} and D can be given by

$$D_{eff} = \frac{D}{\left[1 + pK_t \ln(\frac{D}{D_0})\right]} \qquad [7]$$

Fig. 12 gives D_{eff} as a function of D, for the typical values of K_t and D_0 ($K_t = 0.2$ and $D_0 = 1$ μm) taken from Panda *et al.* [83]. The data in Table 3 fall within the region between the red and blue lines. That is, Eq. [7] may be suitable to describe the relationship between D_{eff} and D in processed Fe-Mn-Si based SMAs. Moreover, it is important to note that the austenitic grains are significantly refined by the twin boundaries. In the case of the existence of twin boundaries, the effectiveness of increasing the heating temperature and extending the heating time is too limited to obtain the coarse austenitic grains, especially millimeter-scale ones. As such, it is necessary to explore the new approach coarsening the austenitic grains. Our research group is carrying out the related studies.

6. Conclusions

It is proposed that coarsening austenitic grains is the key prerequisite to achieving giant recovery strains in polycrystalline Fe-Mn-Si based SMAs. To verify this proposal, we carefully investigated the dependence of recovery strains on the austenitic grain-sizes in cast and processed Fe-Mn-Si based SMAs. The following conclusions are summarized below:

(1) Coarse austenitic grains play two roles in achieving the large recovery strains in polycrystalline Fe-Mn-Si based SMAs. The first is that grain boundaries suppress the stress-induced ε martensitic

transformation in their vicinity and so the increment of grain-size leads to decrease of grain boundary density, and thus weakens the suppressive effect of the grain boundaries on the transformation. The second is that multiple orientations of ε martensite nucleate in small grains, whereas a single orientation is dominant in larger grains. Thus coarse austenitic grains are advantageous to introduce single orientation ε martensite and reduce collisions between martensite plates and colonies, especially when the deformation strain is large. This is borne out in practice where the recovery strains of cast 19Mn-20 alloy with coarse austenitic grains of 652 μm were consistently larger than those of cast 19Mn-5 alloy with relatively small austenitic grains of 382 μm, and this advantage increased with increasing deformation strains. Furthermore, the large grained alloy showed a maximum recovery strain of 7.7% while the smaller grain one only reached 5.4%.

(2) A recovery strain of 5.9%, which is the highest published value for solution-treated processed Fe-Mn-Si based SMAs, was obtained by coarsening the austenitic grains through only solution treatment at 1483 K for 360 min in a processed Fe-17Mn-5.5Si-9Cr-5.5Ni-0.12C alloy. However, the effective austenitic grains of 185.5 μm, taking into account the existence of twin boundaries, did not meet the requirement of austenitic grain-sizes for achieving the large recovery strain of above 6%. Thus, the recovery strain was still 5.9% after thermo-mechanical treatment consisting of 10% tensile strain at RT and annealing at 1073 K for 30 min. The above results confirmed that the ceiling of recovery strains is dependent on the austenitic grain-sizes for polycrystalline Fe-Mn-Si based SMAs.

(3) During solution treatment, the effectiveness of increasing the heating temperature and extending the heating time is too limited to obtain the coarse austenitic grains, especially millimeter-scale ones, owing to that the austenitic grains are refined significantly by the introduction of annealing twins. Consequently, recovery strains of the processed polycrystalline Fe-Mn-Si based SMAs could not be raised above 6%.

(4) It is clearly demonstrated that coarsening austenitic grains is key to achieving giant recovery strains in polycrystalline Fe-Mn-Si based SMAs. Therefore, to maximise the giant recovery strains in cast Fe-Mn-Si based SMAs, the casting parameters and the addition of alloying elements must be considered in order to enable such coarse grains to be realized in practice.

the International Visiting Program for Excellent Young Scholars of SCU.

References

[1]   K. Otsuka, C.M. Wayman, Shape Memory Materials, first ed., Cambridge University Press, United Kingdom, 1998.

[2]   Y. Tanaka, Y. Himuro, R. Kainuma, Y. Sutou, T. Omori, K. Ishida, Ferrous polycrystalline shape-memory alloy showing huge superelasticity, Science 327 (2010) 1488–1490.

[3]   T. Omori, K. Ando, M. Okano, X. Xu, Y. Tanaka, I. Ohnuma, R. Kainuma, K. Ishida, Superelastic effect in polycrystalline ferrous alloys, Science 333 (2011) 68–71.

[4]   Y. Song, X. Chen, V. Dabade, T.W. Shield, R.D. James, Enhanced reversibility and unusual microstructure of a phase-transforming material, Nature 502 (2013) 85–88.

[5]   S. Hao, L. Cui, D. Jiang, X. Han, Y. Ren, J. Jiang, Y. Liu, Z. Liu, S. Mao, Y. Wang, Y. Li, X. Ren, X. Ding, S. Wang, C. Yu, X. Shi, M. Du, F. Yang, Y. Zheng, Z. Zhang, X. Li, D.E. Brown, J. Li, A Transforming Metal Nanocomposite with Large Elastic Strain, Low Modulus, and High Strength, Science 339 (2013) 1191–1194.

[6]   C. Chluba, W. Ge, R. Lima de Miranda, J. Strobel, L. Kienle, E. Quandt, M. Wuttig, Ultralow-fatigue shape memory alloy films, Science 348 (2015) 1004–1007.

[7]   J. Van Humbeeck, Shape memory alloys: a material and a technology, Adv. Eng. Mater. (2001) 837–850.

[8]   K. Otsuka, T. Kakeshita, Science and technology of shape-memory alloys: new development, MRS Bull. (2002) 91–100.

[9]   W.M. Huang, Z. Ding, C.C. Wang, J. Wei, Y. Zhao, H. Purnawali, Shape memory materials, Mater. Today 13 (2010) 54–61.

[10]   S. Barbarino, E.I. Saavedra Flores, R.M. Ajaj, I. Dayyani, M.I. Friswell, A review on shape memory alloys with applications to morphing aircraft, Smart Mater. Struct. 23 (2014) 63001.

[11]   J. Mohd Jani, M. Leary, A. Subic, M.A. Gibson, A review of shape memory alloy research, applications and opportunities, Mater. Des. 56 (2014) 1078–1113.

[12]   T. Sawaguchi, T. Maruyama, H. Otsuka, A. Kushibe, Y. Inoue, K. Tsuzaki, Design concept and applications of Fe-Mn-Si-based alloys-from shape-memory to seismic response control, Mater. Trans. 57 (2016) 283–293.

[13] S. Miyszaki, K. Otsuka, Y. Suzuki, Transformation pseudoelasticity and deformation behavior in a Ti-50.6at%Ni alloy, Scr. Metall. 15 (1981) 287–292.

[14] H.C. Lin, K.M. Lin, Y.C. Chuang, T.S. Chou, Welding characteristics of Fe-30Mn-6Si and Fe-30Mn-6Si-5Cr shape memory alloys, J. Alloys Compd. 306 (2000) 186–192.

[15] A. Sato, H. Kubo, T. Maruyama, Mechanical properties of Fe-Mn-Si based SMA and the application, Mater. Trans. 47 (2006) 571–579.

[16] A. V. Druker, A. Perotti, I. Esquivel, J. Malarría, A manufacturing process for shaft and pipe couplings of Fe-Mn-Si-Ni-Cr shape memory alloys, Mater. Des. 56 (2014) 878–888.

[17] A. Sato, E. Chishima, K. Soma, T. Mori, Shape memory effect in $\gamma \rightleftarrows \epsilon$ transformation in Fe-30Mn-1Si alloy single crystals, Acta Metall. 30 (1982) 1177–1183.

[18] H. Otsuka, H. Yamada, T. Maruyama, H. Tanahashi, S. Matsuda, M. Murakami, Effects of alloying additions on Fe-Mn-Si shape memory alloys, ISIJ Int. 30 (1990) 674–679.

[19] N.E. Stanford, D.P. Dunne, Optimization of alloy design and hot rolling conditions for shape memory in Fe-Mn-Si-based alloys, ISIJ Int. 46 (2006) 1703–1711.

[20] A. Druker, A. Baruj, J. Malarría, Effect of rolling conditions on the structure and shape memory properties of Fe-Mn-Si alloys, Mater. Charact. 61 (2010) 603–612.

[21] C. Leinenbach, C. Czaderski, J. Michels, M. Graf, R. Kawalla, Development of rolling technology for an iron-based shape-memory-alloy, Mater. Sci. Forum. 854 (2016) 79–86.

[22] Y.H. Wen, W. Zhang, N. Li, H.B. Peng, L.R. Xiong, Principle and realization of improving shape memory effect in Fe-Mn-Si-Cr-Ni alloy through aligned precipitations of second-phase particles, Acta Mater. 55 (2007) 6526–6534.

[23] A. Sato, T. Mori, Development of a shape memory alloy Fe-Mn-Si, Mater. Sci. Eng. A. 46 (1991) 197–204.

[24] S. Kajiwara, Characteristic features of shape memory effect and related transformation behavior in Fe-based alloys, Mater. Sci. Eng. A. 273–275 (1999) 67–88.

[25] A. Baruj, T. Kikuchi, S. Kajiwara, N. Shinya, Improvement of shape memory properties of NbC containing Fe-Mn-Si based shape memory alloys by simple thermomechanical treatments, Mater. Sci. Eng. A. 378 (2004) 333–336.

[26] H. Otsuka, N. Masahashi, S. Matsuda, Improvement in the shape memory effect of FeMnSi alloys

by the thermomechanical treatment, in: MRS Int. Meet. Adv. Mater., 1989: pp. 451–456.

[27] Y. Watanabe, Y. Mori, A. Sato, Training effect in FeMnSi shape memory alloys, J. Mater. Sci. 28 (1993) 1509–1514.

[28] Y.H. Wen, H.B. Peng, C.P. Wang, Q.X. Yu, N. Li, A novel training-free cast Fe-Mn-Si-Cr-Ni shape memory alloy based on formation of martensite in a domain-specific manner, Adv. Eng. Mater. 13 (2011) 48–56.

[29] L.J. Rong, Y.Y. Li, C.X. Shi, Improvement of shape memory effect in an Fe-Mn-Si-Cr-Ni alloy, Scr. Mater. 34 (1996) 993–998.

[30] D. Wang, D. Liu, Z. Dong, W. Liu, J. Chen, Improvement of shape memory effect by ausforming in Fe-28Mn-6Si-5Cr alloy, Mater. Sci. Eng. A. 315 (2001) 174–179.

[31] Z.Z. Dong, S. Kajiwara, T. Kikuchi, T. Sawaguchi, Effect of pre-deformation at room temperature on shape memory properties of stainless type Fe-15Mn-5Si-9Cr-5Ni-(0.5-1.5)NbC alloys, Acta Mater. 53 (2005) 4009–4018.

[32] N. Stanford, D.P. Dunne, Thermo-mechanical processing and the shape memory effect in an Fe-Mn-Si-based shape memory alloy, Mater. Sci. Eng. A. 422 (2006) 352–359.

[33] C.H. Yang, H.C. Lin, K.M. Lin, H.K. Tsai, Effects of thermo-mechanical treatment on a Fe-30Mn-6Si shape memory alloy, Mater. Sci. Eng. A. 497 (2008) 445–450.

[34] Y.H. Wen, H.B. Peng, D. Raabe, I. Gutierrez-Urrutia, J. Chen, Y.Y. Du, Large recovery strain in Fe-Mn-Si-based shape memory steels obtained by engineering annealing twin boundaries, Nat. Commun. 5 (2014) 4964.

[35] G.X. Wang, H.B. Peng, P.P. Sun, S.L. Wang, Y.H. Wen, Effect of titanium addition on shape memory effect and recovery stress of training-free cast Fe-Mn-Si-Cr-Ni shape memory alloys, Mater. Sci. Eng. A. 657 (2016) 339–346.

[36] S. Allain, J.P. Chateau, O. Bouaziz, S. Migot, N. Guelton, Correlations between the calculated stacking fault energy and the plasticity mechanisms in Fe-Mn-C alloys, Mater. Sci. Eng. A. 387–389 (2004) 158–162.

[37] H. Idrissi, L. Ryelandt, M. Veron, D. Schryvers, P.J. Jacques, Is there a relationship between the stacking fault character and the activated mode of plasticity of Fe-Mn-based austenitic steels?, Scr. Mater. 60 (2009) 941–944.

[38] T.H. Lee, E. Shin, C.S. Oh, H.Y. Ha, S.J. Kim, Correlation between stacking fault energy and deformation microstructure in high-interstitial-alloyed austenitic steels, Acta Mater. 58 (2010) 3173–3186.

[39] H. Ding, H. Ding, D. Song, Z. Tang, P. Yang, Strain hardening behavior of a TRIP/TWIP steel with 18.8% Mn, Mater. Sci. Eng. A. 528 (2011) 868–873.

[40] Y.F. Shen, Y.D. Wang, X.P. Liu, X. Sun, R. Lin Peng, S.Y. Zhang, L. Zuo, P.K. Liaw, Deformation mechanisms of a 20Mn TWIP steel investigated by in situ neutron diffraction and TEM, Acta Mater. 61 (2013) 6093–6106.

[41] R.L. Xiong, H.B. Peng, S.L. Wang, H.T. Si, Y.H. Wen, Effect of stacking fault energy on work hardening behaviors in Fe-Mn-Si-C high manganese steels by varying silicon and carbon contents, Mater. Des. 85 (2015) 707–714.

[42] K. Ogawa, S. Kajiwara, HREM Study of stree-induced transformation structures in an Fe-Mn-Si-Cr-Ni shape memory alloy, Mater. Trans. 34 (1993) 1169–1176.

[43] N. Bergeon, S. Kajiwara, T. Kikuchi, Atomic force microscope study of stress-induced martensite formation and its reverse transformation in a thermomechanically treated Fe-Mn-Si-Cr-Ni alloy, Acta Mater. 48 (2000) 4053–4064.

[44] D. Liu, S. Kajiwara, T. Kikuchi, N. Shinya, D. Wang, W. Liu, Mechanism of the improvement of the shape memory effect by "training" and ausforming in Fe-Mn-Si based shape memory alloys, Mater. Trans. 41 (2000) 593–596.

[45] D.Z. Liu, S. Kajiwara, T. Kikuchi, N. Shinya, Atomic force microscopy study on microstructural changes by "training" in Fe-Mn-Si-based shape memory alloys, Philos. Mag. 83 (2003) 2875–2897.

[46] A. Baruj, T. Kikuchi, S. Kajiwara, TEM observation of the internal structures in NbC containing Fe-Mn-Si-based shape memory alloys subjected to pre-deformation above room temperature, Mater. Sci. Eng. A. 378 (2004) 337–342.

[47] A. Baruj, H. Troiani, The effect of pre-rolling Fe-Mn-Si-based shape memory alloys: Mechanical properties and transmission electron microcopy examination, Mater. Sci. Eng. A. 481–482 (2008) 574–577.

[48] E. Gartstein, A. Rabinkin, On the f.c.c. → h.c.p. phase transformation in high manganese-iron alloys, Acta Metall. 27 (1979) 1053–1064.

[49] H. Li, D. Dunne, N. Kennon, Factors influencing shape memory effect and phase transformation behaviour of Fe-Mn-Si based shape memory alloys, Mater. Sci. Eng. A. 273–275 (1999) 517–523.

[50] K. Tsuzaki, Y. Natsume, Y. Kurokawa, T. Maki, Improvement of the shape memory effect in Fe-Mn-Si alloys by the addition of carbon, Scr. Metall. Mater. 27 (1992) 471–473.

[51] V. V. Bliznuk, V.G. Gavriljuk, G.P. Kopitsa, S. V. Grigoriev, V. V. Runov, Fluctuations of chemical composition of austenite and their consequence on shape memory effect in Fe-Mn-(Si, Cr, Ni, C, N) alloys, Acta Mater. 52 (2004) 4791–4799.

[52] N. Van Caenegem, L. Duprez, K. Verbeken, B.C. De Cooman, Y. Houbaert, D. Segers, Effect of carbon on the shape memory mechanism in FeMnSiCrNi SMAs, ISIJ Int. 47 (2007) 723–732.

[53] C.P. Wang, Y.H. Wen, H.B. Peng, D.Q. Xu, N. Li, Factors affecting recovery stress in Fe-Mn-Si-Cr-Ni-C shape memory alloys, Mater. Sci. Eng. A. 528 (2011) 1125–1130.

[54] C.H. Yang, H.C. Lin, K.M. Lin, W.H. Ho, Effects of carbon content and thermo-mechanical treatment on $Fe_{59}Mn_{30}Si_6Cr_5C_X$ (X=0.015-0.1 mass%) shape memory alloys, Mater. Trans. 49 (2008) 1853–1857.

[55] M. Koyama, T. Sawaguchi, K. Tsuzaki, Si content dependence on shape memory and tensile properties in Fe-Mn-Si-C alloys, Mater. Sci. Eng. A. 528 (2011) 2882–2888.

[56] M. Koyama, T. Sawaguchi, K. Tsuzaki, Microstructure characteristic and its effect on mechanical and shape memory properties in a Fe-17Mn-8Si-0.3C alloy, J. Alloys Compd. 573 (2013) 15–19.

[57] N.Stanford, K.Chen, D.P.Dunne, X.J.Jin, Effect of alloying additions on the SFE , Neél temperature and shape memory effect in Fe-Mn -Si-based alloys, ISIJ Int. 47 (2007) 883–889.

[58] Q. Gu, J. Van Humbeeck, L. Delaey, A review on the martensitic transformation and shape memory effect in Fe-Mn-Si alloys, J. Phys. IV 4 (1994) 135–144.

[59] J. Chen, H.B. Peng, Q. Yang, S.L. Wang, F. Song, Y.H. Wen, Effect of carbon content on shape memory effect of Fe-Mn-Si-Cr-Ni-based alloys at different deformation temperatures, Mater. Sci. Eng. A. 677 (2016) 133–139.

[60] S. Kajiwara, D. Liu, T. Kikuchi, N. Shinya, Remarkable improvement of shape memory effect in Fe-Mn-Si based shape memory alloys by producing NbC precipitates, Scr. Mater. 44 (2001) 2809–2814.

[61] H. Kubo, K. Nakamura, S. Farjami, T. Maruyama, Characterization of Fe-Mn-Si-Cr shape memory

alloys containing VN precipitates, Mater. Sci. Eng. A. 378 (2004) 343–348.

[62] S. Farjami, K. Hiraga, H. Kubo, Crystallography and elastic energy analysis of VN precipitates in Fe-Mn-Si-Cr shape memory alloys, Acta Mater. 53 (2005) 419–431.

[63] Z. Dong, U.E. Klotz, C. Leinenbach, A. Bergamini, C. Czaderski, M. Motavalli, A novel Fe-Mn-Si shape memory alloy with improved shape recovery properties by VC precipitation, Adv. Eng. Mater. 11 (2009) 40–44.

[64] C. Leinenbach, H. Kramer, C. Bernhard, D. Eifler, Thermo-mechanical properties of an Fe-Mn-Si-Cr-Ni-VC shape memory alloy with low transformation temperature, Adv. Eng. Mater. 14 (2012) 62–67.

[65] N. Stanford, D.P. Dunne, Effect of NbC and TiC precipitation on shape memory in an iron-based alloy, J. Mater. Sci. 41 (2006) 4883–4891.

[66] H.B. Peng, J. Chen, S.L. Wang, Y.H. Wen, Effect of carbon addition on recovery behavior of trained Fe-Mn-Si based shape memory alloys, Adv. Eng. Mater. 17 (2015) 205–210.

[67] H.B. Peng, F. Song, S.L. Wang, C.Y. Zhang, Y.H. Wen, Role of carbon in improving the shape memory effect of Fe-Mn-Si-Cr-Ni alloys by thermo-mechanical treatments, Smart Mater. Struct. 24 (2015) 55010.

[68] H.B. Peng, G.X. Wang, Y.Y. Du, S.L. Wang, J. Chen, Y.H. Wen, A novel training-free processed Fe-Mn-Si-Cr-Ni shape memory alloy undergoing δ → γ phase transformation, Metall. Mater. Trans. A Phys. Metall. Mater. Sci. 47 (2016) 1–7.

[69] G.X. Wang, H.B. Peng, C.Y. Zhang, S.L. Wang, Y.H. Wen, Relationship among grain size, annealing twins and shape memory effect in Fe-Mn-Si based shape memory alloys, Smart Mater. Struct. 25 (2016) 75013.

[70] H.B. Peng, Y.H. Wen, Y.Y. Du, Q.X. Yu, Q. Yang, Effect of manganese on microstructures and solidification modes of cast Fe-Mn-Si-Cr-Ni shape memory alloys, Metall. Mater. Trans. B Process Metall. Mater. Process. Sci. 44 (2013) 1137–1143.

[71] Y.Y. Du, H.B. Peng, J. Chen, Y.H. Wen, S.L. Wang, Microstructures of cast Fe-Mn-Si-Cr-Ni shape memory alloys characterized by metallography, Pract. Metallogr. 51 (2014) 107–126.

[72] Y.H. Wen, H.B. Peng, P.P. Sun, G. Liu, N. Li, A novel training-free cast Fe-18Mn-5.5Si-9.5Cr-4Ni shape memory alloy with lathy delta ferrite, Scr. Mater. 62 (2010) 55–58.

[73] Y. Sutou, T. Omori, K. Yamauchi, N. Ono, R. Kainuma, K. Ishida, Effect of grain size and texture on pseudoelasticity in Cu-Al-Mn-based shape memory wire, Acta Mater. 53 (2005) 4121–4133.

[74] J. Campbell, Castings, second ed., Butterworth-Heinemann, Oxford, 2003.

[75] H.B. Peng, Y.H. Wen, Y.Y. Du, J. Chen, Q. Yang, A new set of Creq and Nieq equations for predicting solidification modes of cast austenitic Fe-Mn-Si-Cr-Ni shape memory alloys, Metall. Mater. Trans. B Process Metall. Mater. Process. Sci. 45 (2014) 6–11.

[76] J.C. Lippold, D.J. Kotecki, Welding Metallurgy and Weldability of Stainless Steels, first ed., John Wiley & Sons, Hoboken, 2005.

[77] M. Andersson, R. Stalmans, J. Ågren, Unified thermodynamic analysis of the stress-assisted γ→ε martensitic transformation in Fe-Mn-Si alloys, Acta Mater. 46 (1998) 3883–3891.

[78] O. Matsumura, S. Furusako, T. Sumi, T. Furukawa, H. Otsuka, Improvement of shape memory effect due to low-finishing-temperature hot-rolling in an Fe-28Mn-6Si-5Cr alloy, Mater. Sci. Eng. A. 272 (1999) 459–462.

[79] T. Sawaguchi, T. Kikuchi, S. Kajiwara, The pseudoelastic behavior of Fe-Mn-Si-based shape memory alloys containing Nb and C, Smart Mater. Struct. 14 (2005) S317–S322.

[80] H.C. Lin, S.K. Wu, Y.T. Peng, T.C. Cheng, K.M. Lin, Pseudoelasticity of thermo-mechanically treated Fe-Mn-Si-Cr-Ta alloys, J. Alloys Compd. 577 (2013) 1–6.

[81] W.J. Lee, B. Weber, G. Feltrin, C. Czaderski, M. Motavalli, C. Leinenbach, Phase transformation behavior under uniaxial deformation of an Fe-Mn-Si-Cr-Ni-VC shape memory alloy, Mater. Sci. Eng. A. 581 (2013) 1–7.

[82] W. Tasaki, T. Sawaguchi, I. Nikulin, K. Sekido, K. Tsuchiya, Effect of deformation temperature on low-cycle fatigue properties of Fe-28Mn-6Si-5Cr shape memory alloy, Mater. Trans. 57 (2016) 639–646.

[83] C.S. Pande, B.B. Rath, M.A. Imam, Effect of annealing twins on Hall-Petch relation in polycrystalline materials, Mater. Sci. Eng. A. 367 (2004) 171–175.

[84] S.M. Ueland, C.A. Schuh, Grain boundary and triple junction constraints during martensitic transformation in shape memory alloys, J. Appl. Phys. 114 (2013) 53503.

[85] S. Takaki, H. Nakatsu, Y. Tokunaga, Effects of austenite grain size on ε martensitic transformation in Fe-15mass%Mn alloy, Mater. Trans. 34 (1993) 489–495.

[86]   J.H. Jun, C.S. Choi, Variation of stacking fault energy with austenite grain size and its effect on the Ms temperature of γ→ε martensitic transformation in Fe-Mn alloy, Mater. Sci. Eng. A. 257 (1998) 353–356.

[87]   M. Umemoto, W.S. Owen, Effects of austenitising temperature and austenite grain size on the formation of athermal martensite in an Iron-Nickel and an Iron-Nickel-Carbon alloy, Metall. Trans. 5 (1974) 2041–2046.

[88]   G.S. Brofman, P.J., Ansell, On the effect of fine grain size on the Ms temperature in Fe-27Ni-0.025C alloys, Metall. Mater. Trans. A. 14 (1983) 2–4.

[89]   C. Hayzelden, B. Cantor, The martensite transformation in Fe-Ni-C alloys, Acta Metall. 34 (1986) 233–242.

[90]   K. Seki, H. Kura, T. Sato, T. Taniyama, Size dependence of martensite transformation temperature in ferromagnetic shape memory alloy FePd, J. Appl. Phys. 103 (2008) 063910.

[91]   D.N. Adnyana, Effect of grain size on transformation temperatures in a grain- refined, copper-based, shape-memory Alloy, Metallography. 18 (1985) 187–196.

[92]   K. Mukunthan, L.C. Brown, Preparation and properties of fine grain β-CuAlNi strain-memory alloys, Metall. Trans. A. 19 (1988) 2921–2929.

[93]   C. López del Castillo, B.G. Mellor, M.L. Bálzquez, C. Gómez, The influence of composition and grain size on the martensitic transformation temperatures of Cu-Ai-Mn shape memroy alloys, Scr. Metall. 21 (1987) 1711–1716.

[94]   T. Waitz, T. Antretter, F.D. Fischer, H.P. Karnthaler, Size effects on martensitic phase transformations in nanocrystalline NiTi shape memory alloys, Mater. Sci. Technol. 24 (2008) 934–940.

[95]   A. Sato, T. Masuya, M. Morishita, S. Kumai, A. Inoue, Strengthening of Fe-Mn-Si based shape memory alloys by grain size refinement, Mater. Sci. Forum. 327–328 (2000) 223–226.

[96]   K.K. Jee, W.Y. Jang, Y.H. Chung, M.C. Shin, Effect of microstructure on shape-memory effect in Fe-32Mn-6.5Si alloy, Mater. Sci. Forum. 394–395 (2002) 423–426.

[97]   G.N. Sure, L.C. Brown, The mechanical properties of grain refined β-CuAlNi strain-memory alloys, Metall. Trans. A. 15 (1984) 1613–1621.

[98]   M. Somerday, R.J. Comstock, J.A. Wert, Effect of grain size on the observed pseudoelastic

behavior of a Cu-Zn-Al shape memory alloy, Metall. Mater. Trans. A. 28 (1997) 2335–2341.

[99] S. Montecinos, A. Cuniberti, A. Sepúlveda, Grain size and pseudoelastic behaviour of a Cu-Al-Be alloy, Mater. Charact. 59 (2008) 117–123.

[100] T. Sawaguchi, M. Sato, A. Ishida, Grain-size effect on shape-memory behavior of Ti35.0Ni49.7Zr15.4 thin films, Metall. Mater. Trans. A. 35 (2004) 111–119.

[101] C.W. Sinclair, W.J. Poole, Y. Bréchet, A model for the grain size dependent work hardening of copper, Scr. Mater. 55 (2006) 739–742.

[102] S.T. Pisarik, D.C. Van Aken, Thermodynamic driving force of the $\gamma \rightarrow \varepsilon$ transformation and resulting Ms Temperature in high-Mn steels, Metall. Mater. Trans. A Phys. Metall. Mater. Sci. 47 (2015) 1–10.

[103] J.X. Yang, Physical Basis of Metal Plastic Deformation, 1st ed., Metallurgical Industry Press, Beijing, 1988.

[104] A. Sato, E. Chishima, Y. Yamaji, T. Mori, Orientation and composition dependencies of shape memory effect in Fe-Mn-Si alloys, Acta Metall. 32 (1984) 539–547.

[105] J.H. Yang, C.M. Wayman, On secondary variants formed at intersections of ε martensite variants, Acta Metall. Mater. 40 (1992) 2011–2023.

[106] C. Devadas, I. V. Samarasekera, E.B. Hawbolt, The thermal and metallurgical state of steel strip during hot rolling: Part Ⅲ. microstructural evolution, Metall. Trans. A. 22 (1991) 335–349.

[107] L. Rémy, Twin-slip interaction in f.c.c. crystals, Acta Metall. 25 (1977) 711–714.

[108] Z. Dong, T. Kikuchi, T. Sawaguchi, S. Kajiwara, Martensite transformation and shape recovery in pre-deformed Fe-15Mn-5Si-9Cr-5Ni-(0.5-1.5) NbC alloys, Mater. Trans. 47 (2006) 1328–1331.

[109] C.S. Pande, M. a. Imam, B.B. Rath, Study of annealing twins in fcc metals and alloys, Metall. Trans. A. 21 (1990) 2891–2896.

[110] S. Mahajan, Critique of mechanisms of formation of deformation, annealing and growth twins: Face-centered cubic metals and alloys, Scr. Mater. 68 (2013) 95–99.
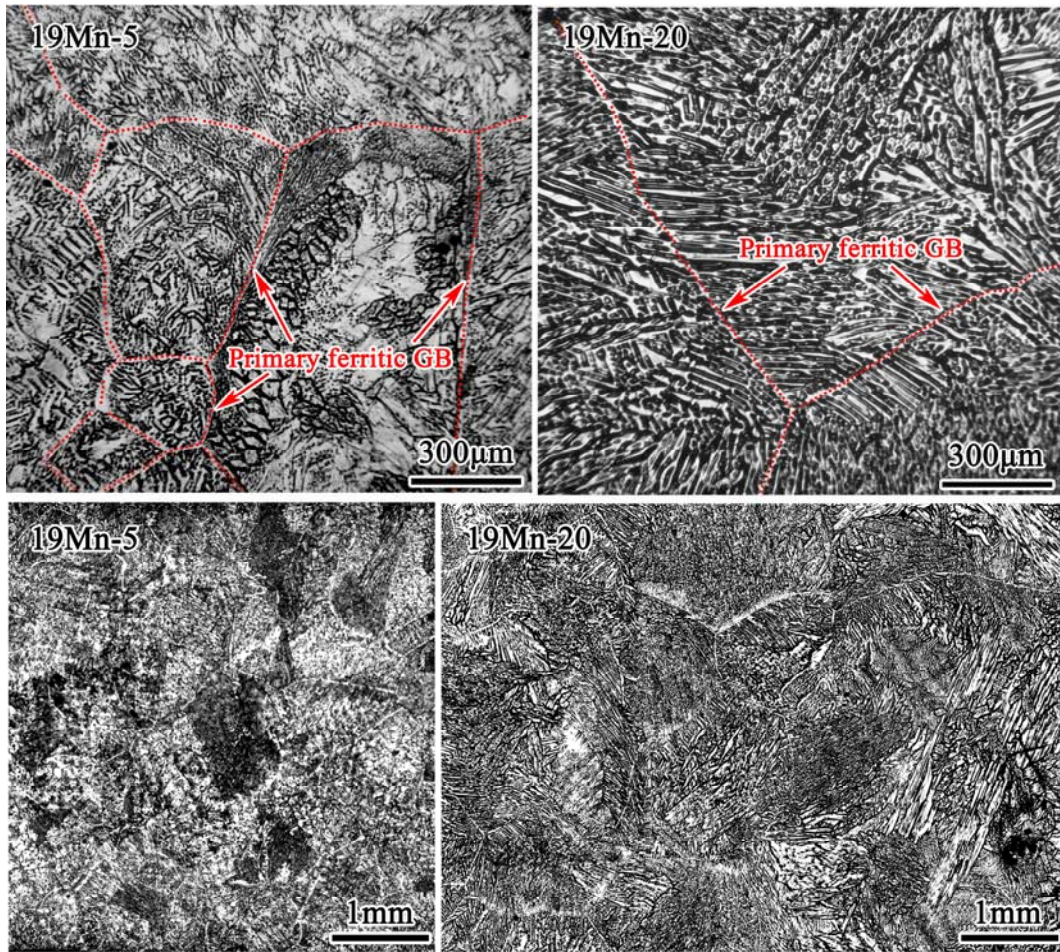
Fig. 1 Ordinary optical micrographs with different magnifications for as-cast 19Mn-5 and 19Mn-20 alloys. Red dotted lines indicate the grain boundaries (GBs) of primary δ ferrite.
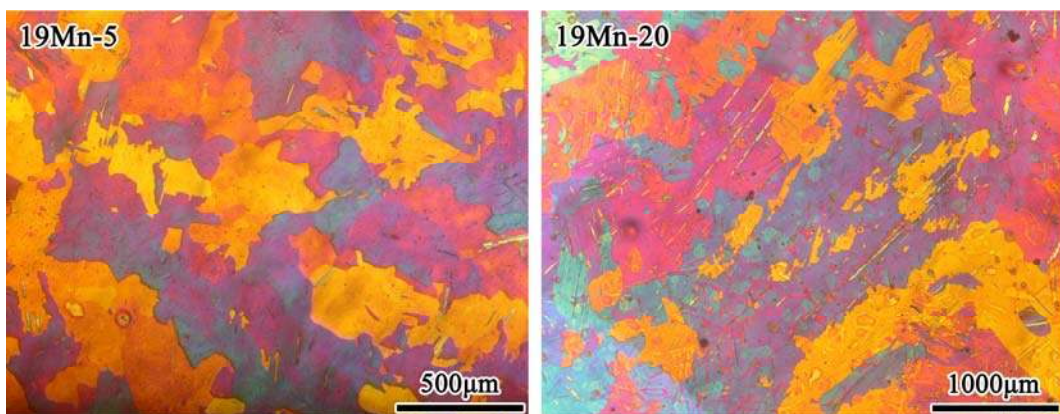

Fig. 2 Color optical micrographs of as-cast 19Mn-5 and 19Mn-20 alloys. Different austenitic grains exhibit different colors.
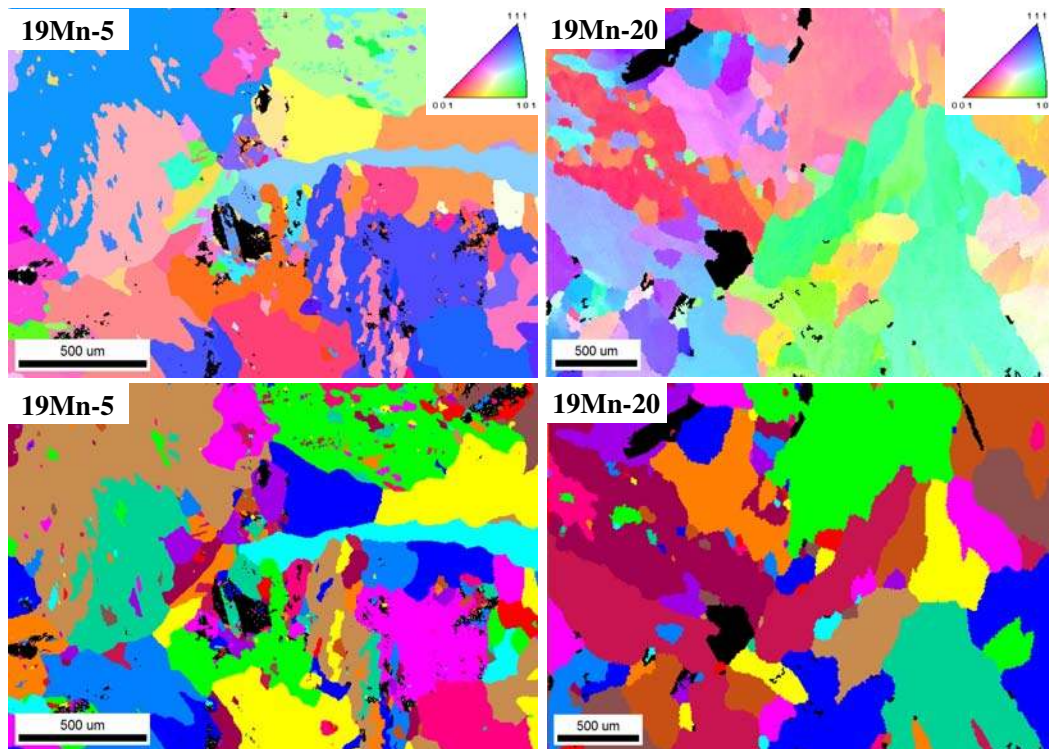
Fig. 3 EBSD austenitic inverse pole figures and corresponding grain maps of as-cast 19Mn-5 and 19Mn-20 alloys after annealed at 873 K for 30 min.
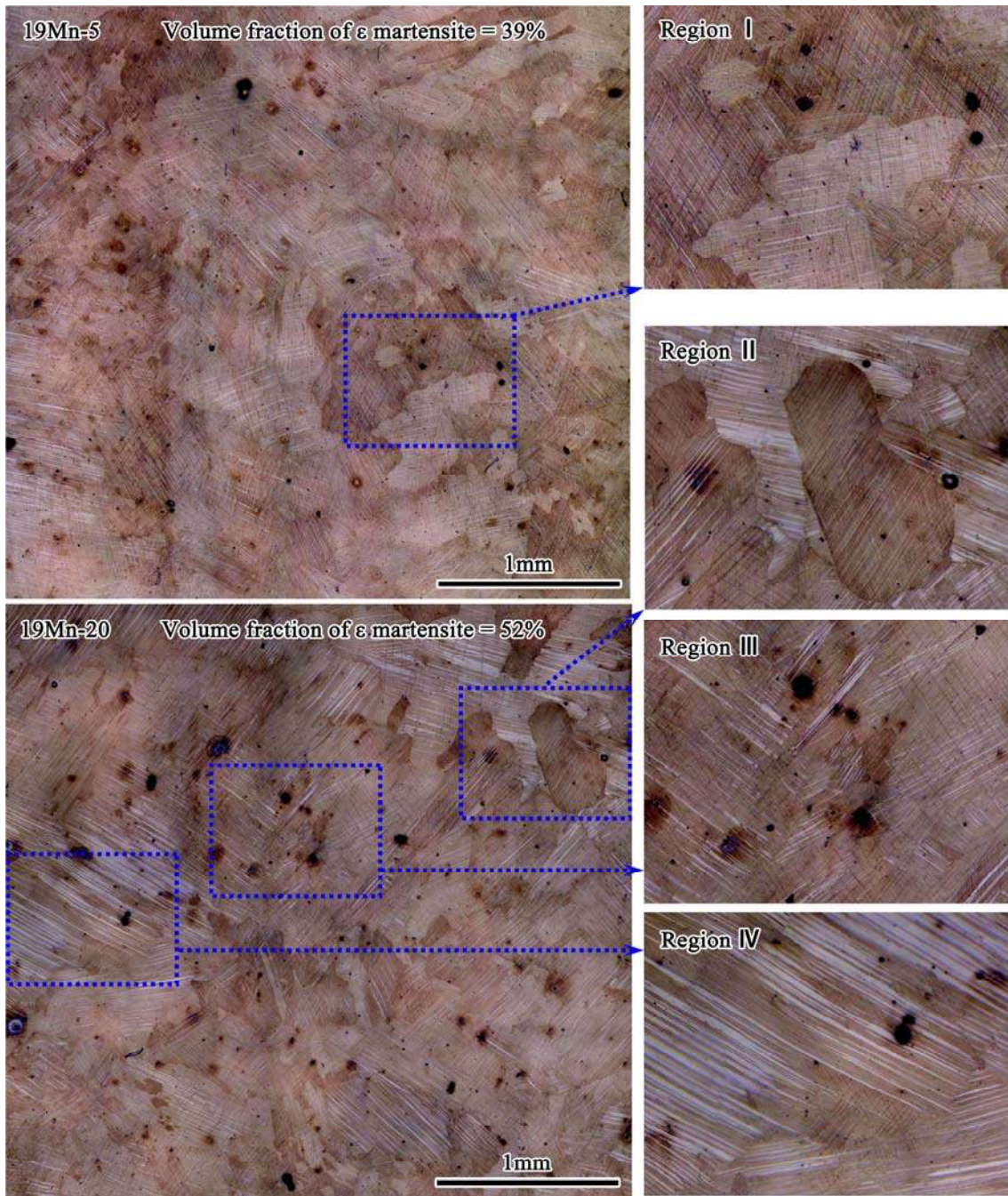
Fig. 4 Color optical micrographs of as-cast 19Mn-5 and 19Mn-20 alloys annealed at 873 K for 30 min after 5% tensile deformation at M_s + 10 K.
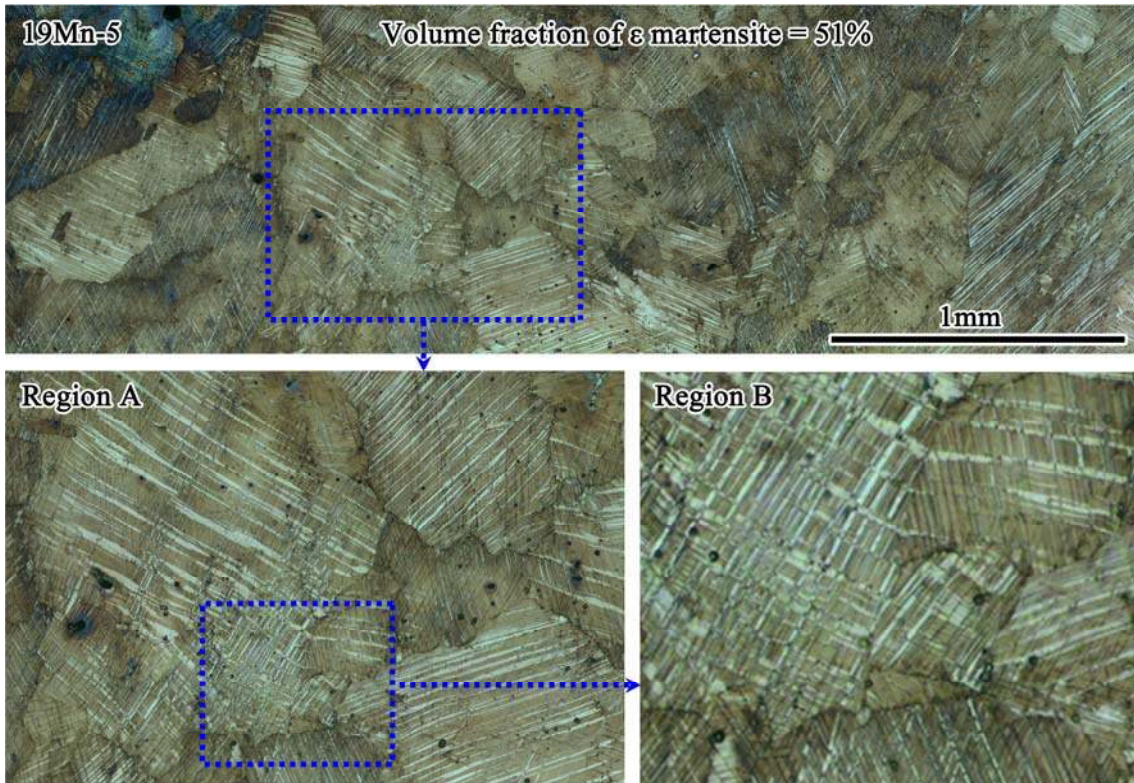
Fig. 5 Color optical micrographs of as-cast 19Mn-5 alloy annealed at 873 K for 30 min after 10% tensile deformation at $M_s + 10$ K.
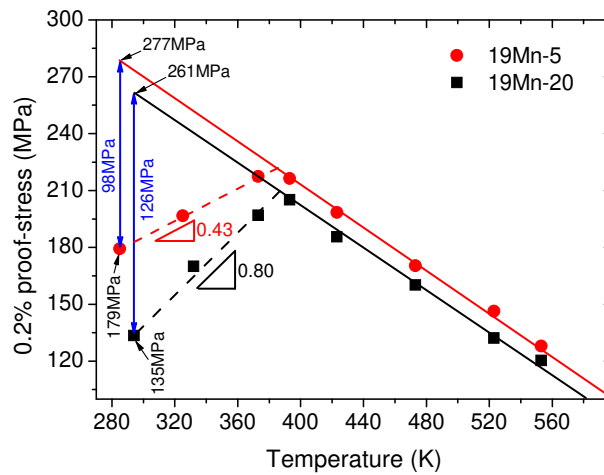
Fig. 6 Color optical micrographs of as-cast 19Mn-20 alloy annealed at 873 K for 30 min after 10% tensile deformation at M_s +10 K.

Fig. 7 Temperature dependence of 0.2% proof-stress for as-cast 19Mn-5 and 19Mn-20 alloys annealed at 873 K for 30 min. Solid lines represent the critical stress for plastic yielding associated with irreversible slip, and dashed lines represent the critical stress for inducing martensitic transformation. $\Delta\sigma$ is plotted in blue for both alloys as the difference between the solid and dotted lines at M_s + 10 K.
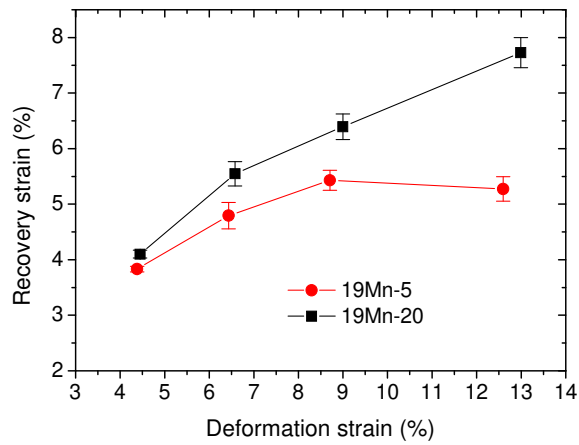
Fig. 8 Recovery strains as a function of deformation strains for as-cast 19Mn-5 and 19Mn-20 alloys annealed at 873 K for 30 min when the deformation temperatures were $M_s + 10$ K.
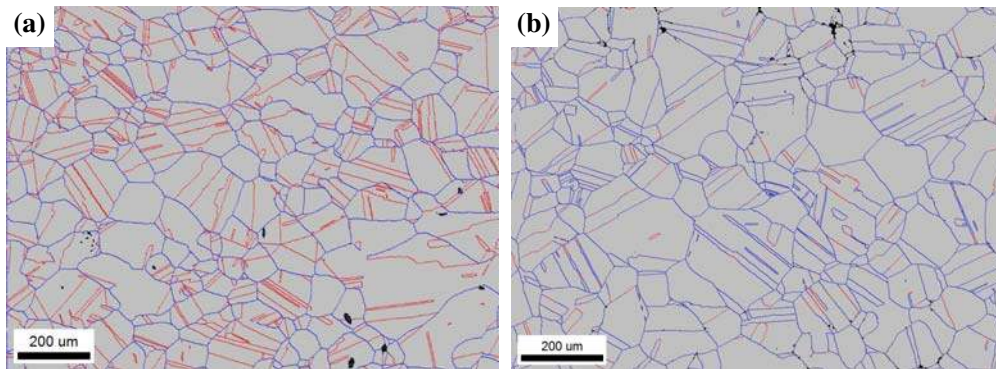

Fig. 9 Austenitic EBSD phase maps of processed Fe-17Mn-5.5Si-9Cr-5.5Ni-0.12C alloy subjected to solution treatment at 1373 K for 30 min (a) and subsequent TMT (b). The blue lines correspond to high-angle boundaries with the misorientation larger than 15 degrees. The red lines correspond to annealing twin boundaries.
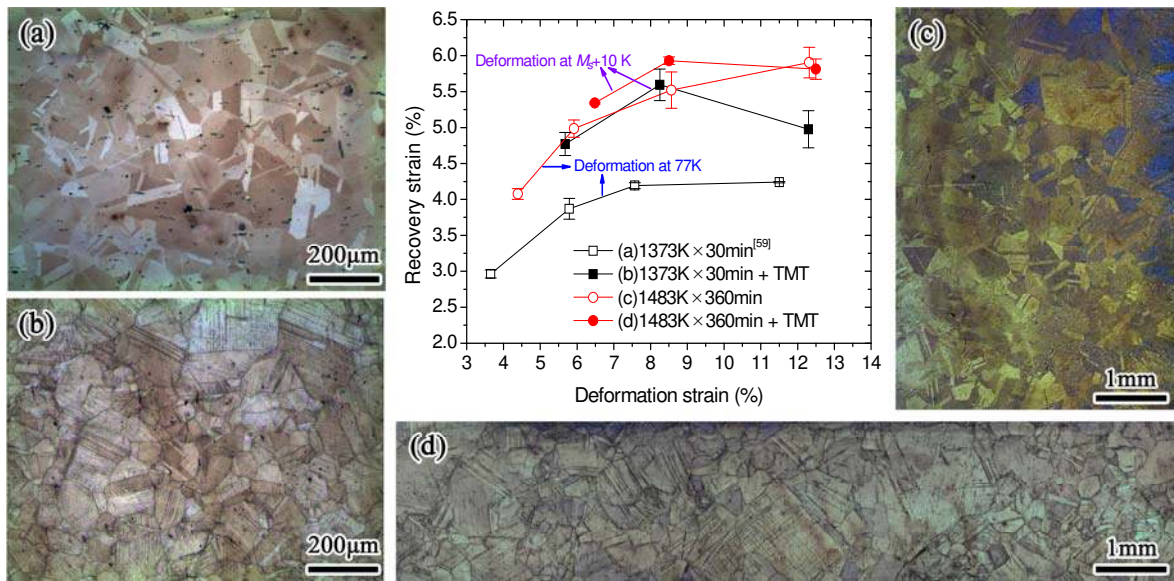
Fig. 10 Recovery strains as a function of deformation strains as well as color optical micrographs for solution treated Fe-17Mn-5.5Si-9Cr-5.5Ni-0.12C alloy at 1373 K for 30 min and 1483 K for 360 min, respectively, as well as ones after TMT.
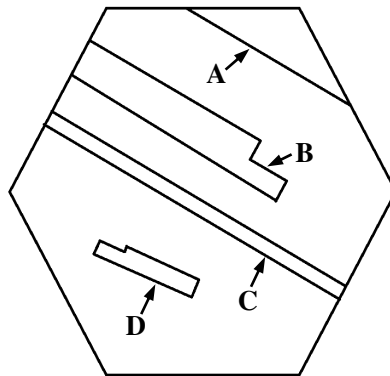

Fig. 11 Schematic sketch for four types of annealing twins in FCC crystals.
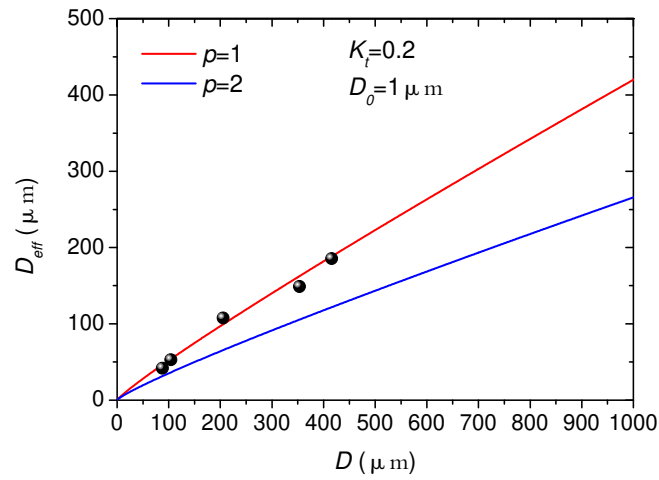
Fig. 12 Relationship between the effective austenitic grain-size considering twin boundaries (D_{eff}) and the austenitic grain-size without considering twin boundaries (D) according to Eq. [7]. The data indicated by black spheres are from Table 3. The red and blue lines are for two different values of p in Eq. [7].

Table 1 Chemical compositions of cast and processed Fe-Mn-Si-Cr-Ni SMAs

Shape memory alloys	Chemical compositions (wt%)					
	Mn	Si	Cr	Ni	C	Fe
Cast 19Mn-5 alloy Cast 19Mn-20 alloy	18.54	5.70	8.91	4.45	0.008	Bal.
Processed alloy	16.99	5.59	9.28	5.67	0.116	Bal.

Table 2 Phase transformation temperatures of as-cast 19Mn-5 and 19Mn-20 alloys before and after annealed at 873 K for 30 min

Alloys	Heat treatment	Phase transformation temperatures (K)		
		M_s	A_s	A_f
19Mn-5	As-cast	262	343	388
	Annealing at 873 K	275	359	400
19Mn-20	As-cast	263	355	405
	Annealing at 873 K	284	361	406

Table 3 Austenitic grain-sizes of processed Fe-17Mn-5.5Si-9Cr-5.5Ni-0.12C alloy subjected to different heat-treatments

Solution treatments	Thermo-mechanical treatment	D_{eff}^{*} (μm)	D^{**} (μm)
1373 K×30 min	/	41.7	87.9
1373 K×30 min	10% + 1073 K×30 min	53.1	104.2
1473 K×120 min	/	107.8	205.6
1483 K×360 min	/	149.0	353.5
1483 K×360 min	10% + 1073 K×30 min	185.5	415.8

*Twin boundaries or distorted twin boundaries were considered as grain boundaries.
**Twin boundaries or distorted twin boundaries were not considered as grain boundaries.

Table 4 Phase transformation temperatures of processed Fe-17Mn-5.5Si-9Cr-5.5Ni-0.12C alloy subjected to TMT after solution treatments at 1373 K for 30 min and 1483 K for 360 min, respectively.

Heat treatments	Phase transformation temperatures (K)		
	M_s	A_s	A_f
1373 K×30 min + TMT	217	358	408
1483 K×360 min + TMT	219	343	385